J. Fluid Mech. (2007), *vol.* 584, *pp.* 397–413.
doi:10.1017/S0022112007006544 Printed in the United Kingdom

Turbulent spots in the asymptotic suction boundary layer

ORI LEVIN AND DAN S. HENNINGSON

Department of Mechanics, Royal Institute of Technology, SE-100 44 Stockholm, Sweden

(Received 31 March 2006 and in revised form 19 March 2007)

Amplitude thresholds for transition of localized disturbances, their breakdown to turbulence and the development of turbulent spots in the asymptotic suction boundary layer are studied using direct numerical simulations. A parametric study of the horizontal scales of the initial disturbance is performed and the disturbances that lead to the highest growth under the conditions investigated are used in the simulations. The Reynolds-number dependence of the threshold amplitude of a localized disturbance is investigated for $500 \leqslant Re \leqslant 1200$, based on the free-stream velocity and the displacement thickness. It is found that the threshold amplitude scales as $Re^{-1.5}$ for the considered Reynolds numbers. For $Re \leqslant 367$, the localized disturbance does not lead to a turbulent spot and this provides an estimate of the critical Reynolds number for the onset of turbulence. When the localized disturbance breaks down to a turbulent spot, it happens through the development of hairpin and spiral vortices. The shape and spreading rate of the turbulent spot are determined for $Re = 500$, 800 and 1200. Flow visualizations reveal that the turbulent spot takes a bullet-shaped form that becomes more distinct for higher Reynolds numbers. Long streaks extend in front of the spot and in its wake a calm region exists. The spreading rate of the turbulent spot is found to increase with increasing Reynolds number.

1. Introduction

In natural transition, the breakdown to turbulence typically starts in isolated regions initiated by disturbances present in the laminar flow. These turbulent spots grow in size as they propagate downstream and merge to form a fully developed turbulent flow. Turbulent spots were first observed by Emmons (1951) in shallow water flowing down an inclined plate. Since then, turbulent spots and their development have been investigated extensively in channel flows and boundary layers.

The early experimental work of turbulent spots in boundary layers has been reviewed by Riley & Gad-el-Hak (1985). Flow visualizations of Elder (1960) and Cantwell, Coles & Dimotakis (1978) reveal that the turbulent spot in the boundary layer over a flat plate takes the form of an arrowhead with its tip pointing downstream. The leading edge develops an overhang over the laminar boundary layer. Behind the spot, a non-turbulent region with streaks can be seen. The laminar flow in the wake of the turbulent spot turns out to be more stable and has been termed a calmed region. The leading and trailing edges propagate at about 90 % and 50 % of the free-stream velocity, respectively, while the lateral spreading is at a half-width angle of about 10° regardless of Reynolds number (Wygnanski, Sokolov & Friedman 1976). As the spot propagates downstream, its height increases at a rate similar to the growth of a turbulent boundary layer. Wygnanski, Haritonidis & Kaplan (1979) observed oblique

wave packets swept at an angle of about 40° near the wingtips of the spot. Whether these waves packets play an important role in the lateral spreading or merely act as passive attendants to the spot has been debated.

The evolution of turbulent spots in boundary layers with pressure gradients has also been investigated. Katz, Seifert & Wygnanski (1990) observed that the rate of growth of the spot is significantly inhibited by a favourable pressure gradient. The familiar arrowhead shape of the spot gave way to a rounded triangular shape with the trailing interface being straight and perpendicular to the free-stream direction. They did not observe wave packets and attributed this to the stability of the laminar flow. With an adverse pressure gradient, the trend is the opposite, as observed by Seifert & Wygnanski (1995). The rate of growth of turbulent spots, especially the lateral growth, is enhanced by an adverse pressure gradient as well as the interaction of the spot with the wave packet trailing it.

There are very few simulations of turbulent spots in boundary layers. The first direct numerical simulation (DNS) of a spot that was taken far enough in time to make comparisons with experiments was performed by Henningson, Spalart & Kim (1987) for a temporally growing Blasius boundary layer. Singer (1996) looked more into details of the substructures within a young turbulent spot by means of DNS of a spatially growing Blasius boundary layer. In these simulations, the spot assumed the well-known shape of an arrowhead with its characteristic overhang of the leading edge, but wave packets were not observed.

In plane Poiseuille flow, the spot develops the shape of a reverse arrowhead as can be seen in flow visualizations by Carlson, Widnall & Peeters (1982) and Alavyoon, Henningson & Alfredsson (1986). Oblique waves can be seen at the wingtips and streaks extend into the interior of the spot throughout its length. Henningson & Alfredsson (1987) further investigated oblique waves. Contrary to spots in the flat-plate boundary layer, the spreading rates in the streamwise and spanwise directions are found to depend on the Reynolds number (Alavyoon *et al.* 1986). The only simulation of a turbulent spot in plane Poiseuille flow was performed by Henningson & Kim (1991). Their obtained spot had a very similar shape to that observed in laboratory flows and oblique waves existed at the wingtips.

For turbulent spots in plane Couette flow, the simulations of Lundbladh & Johansson (1991) preceded the experiments of Tillmark & Alfredsson (1992) and Dauchot & Daviaud (1995). In both the simulations and the experiments, the spot assumed an elliptical shape that evolved towards a circular shape as it propagated downstream. Moreover, the lateral spreading rate increased with increasing Reynolds number for low Reynolds numbers, but levelled off to a constant rate at high Reynolds numbers corresponding to a half-width angle of 13° in the simulations and 11° in the experiments of Tillmark & Alfredsson (1992). In the experiments, waves with the wave crests aligned in the streamwise direction were observed at the spanwise edges of the spots. These waves were not observed in the simulations.

There have been many investigations of turbulent spots in wall-bounded flows, mostly experimental studies, but also simulations (Mathew & Das 2000). However, nothing has been reported on turbulent spots in the asymptotic suction boundary layer (ASBL). Boundary layers subjected to suction at the wall are interesting flow cases with applications in the area of control (Joslin 1998; Balakumar & Hall 1999; Pralits, Hanifi & Henningson 2002; Zuccher, Luchini & Bottaro 2004). The ASBL is stable to infinitesimal disturbances below a critical Reynolds number of 54 370, based on the free-stream velocity and the displacement thickness (Hocking 1975). However, a transient disturbance growth may occur for much lower Reynolds numbers (Fransson

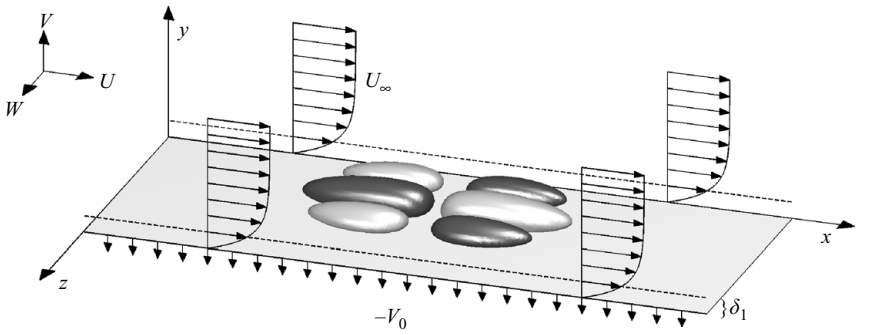

FIGURE 1. The asymptotic suction boundary layer and a localized disturbance with dark grey indicating upward moving fluid and light grey fluid moving downward.

& Alfredsson 2003; Fransson & Corbett 2003; Yoshioka, Fransson & Alfredsson 2004; Byström, Levin & Henningson 2007). Levin, Davidsson & Henningson (2005) reported breakdown to turbulence in the ASBL at a Reynolds number of 500. Mariani, Spalart & Kollmann (1993) reported sustained turbulence in the suction turbulent boundary layer for a corresponding Reynolds number as low as 278. At the time of writing this paper, experiments of turbulent spots in the ASBL are being performed in the MTL wind-tunnel at KTH Mechanics in Stockholm (J. H. M. Fransson, personal communication).

In the present study, threshold amplitudes of localized disturbances, their breakdown and the development of turbulent spots in the ASBL are carried out by means of DNS. In § 2, the numerical method is presented as well as a parametric study of the localized disturbance. In § 3, the results are organized as follows: amplitude thresholds are presented in § 3.1, vortical structures within a transitional localized disturbance are visualized in § 3.2 and the development of turbulent spots is investigated in § 3.3. Finally, conclusions are drawn in § 4.

2. Numerical details

2.1. *Base flow and scaling*

Consider a boundary layer over an infinite wall with permeable properties and with suction applied under it (figure 1). The coordinates in the streamwise, wall-normal and spanwise directions are denoted x, y and z, respectively. The corresponding velocity components are $\boldsymbol{U} = (U, V, W)$. Lengths are scaled by the displacement thickness δ_1 and velocities are scaled by the free-stream velocity U_∞. The units of time t are δ_1/U_∞. The Reynolds number is defined as $Re = U_\infty\delta_1/\nu$, where ν is the kinematic viscosity of the fluid. When uniform wall-normal suction, with velocity $-V_0$, is applied at the wall, the displacement thickness, shown as the dashed lines in figure 1, becomes constant over the wall. The asymptotic suction profile can be experimentally obtained after some evolution region (Fransson & Alfredsson 2003). The ASBL is an analytical solution to the Navier–Stokes equations. It was first derived by Griffith & Meredith (1936) and can be written as

$$\boldsymbol{U}_0 = (1 - \exp(-y), -V_0, 0). \tag{2.1}$$

The analytical solution allows the displacement thickness to be calculated exactly, $\delta_1 = \nu/V_0^*$ and the Reynolds number to be expressed as the velocity ratio, $Re = U_\infty/V_0^*$, where $-V_0^*$ is the dimensional suction velocity.

2.2. *DNS techniques*

The numerical code (see Lundbladh *et al.* 1999) uses spectral methods to solve the three-dimensional time-dependent incompressible Navier–Stokes equations. The discretization in the streamwise and spanwise directions makes use of Fourier series expansions, which enforce periodic solutions. The discretization in the wall-normal direction is represented with Chebyshev polynomial series. A pseudospectral treatment of the nonlinear terms is used. The time advancement is a second-order Crank–Nicolson method for the linear terms and a four-step low-storage third-order Runge–Kutta method for the nonlinear terms. Aliasing errors arising from the evaluation of the pseudospectrally convective terms are removed by dealiasing by padding and truncation using the 3/2-rule when the fast Fourier transforms are calculated in the wall-parallel planes. In the wall-normal direction, it is found that increasing the resolution is more efficient than the use of dealiasing. The code can be used for both temporal and spatial simulations. In the latter case, a fringe region (Nordström, Nordin & Henningson 1999) is added to the downstream end of the physical domain, in which the outgoing flow is forced to its initial state. However, when studying parallel flows, such as the ASBL with a localized disturbance, the advantage of omitting the fringe region can be used.

The numerical code does not allow for uniform flow through the lower and upper boundaries. However, the wall-normal suction in the ASBL can be moved from the boundary conditions to the governing equations (see Levin *et al.* 2005). Hence, instead of solving the Navier–Stokes equations for V with the boundary condition $V = -V_0$, the same solution can be obtained by solving for $V - V_0$ with the boundary condition $V = 0$.

At the wall, no-slip boundary conditions are specified and at the upper edge of the computational box, a generalized boundary condition is applied in Fourier space with different coefficients for each wavenumber. The condition represents a potential-flow solution decaying away from the upper edge of the computational box and decreases the required box height by damping the higher frequencies rather than forcing the disturbance velocities to a rapid decay. In the horizontal directions, periodic boundary conditions are used.

2.3. *Disturbance generation*

The present numerical implementation provides several possibilities for disturbance generation. Disturbances can be included in the flow by a body force, by blowing and suction at the wall through non-homogeneous boundary conditions and by adding them in the initial velocity field. In order to produce a turbulent spot, a localized disturbance is superposed to the ASBL in the initial velocity field. This type of disturbance is centred around a pair of oblique waves, in the streamwise-spanwise wavenumber plane, consisting of two counter-rotating vortex pairs, (figure 1). This type of initial disturbance has been used in earlier studies of transient growth and transition in channel flows (Henningson, Lundbladh & Johansson 1993) and boundary layers (Breuer & Haritonidis 1990; Breuer & Landahl 1990; Bech, Henningson & Henkes 1998). In terms of a streamfunction, it is defined by

$$\psi = A\bar{x}\bar{y}^3\bar{z}\exp(-\bar{x}^2 - \bar{y}^2 - \bar{z}^2), \tag{2.2}$$

Re	*A*	$L_x \times L_y \times L_z$	$N_x \times N_y \times N_z$	End time
500	0.08	$100 \times 15 \times 40$	$200 \times 101 \times 160$	200
800	0.05	$100 \times 15 \times 40$	$320 \times 161 \times 256$	200
1200	0.03	$100 \times 15 \times 40$	$480 \times 241 \times 384$	200

TABLE 1. Flow and box parameters for resolution checks.

where $\bar{x} = x/l_x$, $\bar{y} = y/l_y$ and $\bar{z} = z/l_z$. The velocity components are given by $(u, v, w) = (0, -\psi_z, \psi_y)$ and normalized so that the amplitude A is given by the maximum absolute value of the wall-normal disturbance velocity. The energy of the disturbance is defined by

$$E = \tfrac{1}{2} \int (u^2 + v^2 + w^2)\, \mathrm{d}x\, \mathrm{d}y\, \mathrm{d}z. \tag{2.3}$$

When studying the development of turbulent spots, apart from the localized disturbance, random noise is added to the initial velocity field in order to break up symmetries. The noise is in the form of Stokes modes, i.e. eigenmodes of the flow operator without the convective term. These modes fulfil the equation of continuity and the boundary condition of vanishing velocity at the wall. The introduced noise level is specified with its energy density, that is, the total energy of the noise divided by the volume of the box.

2.4. *Numerical parameters*

Amplitude thresholds for transition and the development of turbulent spots are investigated for three Reynolds numbers, $Re = 500$, 800 and 1200. For each Reynolds number, the resolution is carefully checked for a small test case. Dealiasing is activated in the streamwise and spanwise directions. The amplitude of the localized disturbance, which has the scales $l_x = 10$, $l_y = 1.0$ and $l_z = 5.5$, is about twice as large as the threshold value for the corresponding Reynolds number, resulting in breakdown to a turbulent spot well before the termination time of 200. When evaluating the resolution convergence, the disturbance energy, extreme values of velocity and vorticity components and visual examinations of flow structures are taken into account. It was decided to use the resolutions given in table 1 after comparsion to both coarser and finer grids not given here. The time step is set adaptively to keep the CFL number close to a fixed number. Hence, the time resolution is changed with the spatial resolution and therefore included in the resolution checks. As can be seen in table 1, the resolution in each direction is linearly scaled with the Reynolds number. Moreover, when the box size is increased, the resolution is increased correspondingly to ensure the same number of modes per length unit in each direction. To summarize the above, the number of modes is at least given by $(N_x \times N_y \times N_z) = (L_x Re/250 \times L_y Re/75 + 1 \times L_z Re/125)$, where L_x, L_y and L_z denote the length, height and width of the box, respectively. When searching for the critical Reynolds number, the resolution for $Re = 500$ is used.

Apart from the resolution checks, the size of the box is examined for a few cases. It is found that the required box height decreases with increased Reynolds number. One reason for this could be that lower initial amplitudes of the wall-normal disturbance velocity are used for higher Reynolds numbers. The interaction distance between mirror spots in the spanwise direction is short, resulting in low sensitivity of the box width. On the other hand, the interaction distance in the streamwise direction is longer. The interaction takes the form of bonding between streaks at the front and

trail of mirror spots. For each simulation, the box size is set to fit one spot and avoid interactions between mirror spots during the time simulated.

2.5. *Study of horizontal scales of a localized disturbance*

The influence of the streamwise and spanwise length scales of the localized disturbance is studied. The wall-normal scale is $l_y = 1$ while the horizontal scales l_x and l_z are varied. The Reynolds number is $Re = 500$ and the size of the computational box used for this parametric study is $(L_x \times L_y \times L_z) = (100 \times 15 \times 50)$. In a first attempt to study how the horizontal scales of the initial disturbance affect the development of a turbulent spot, the amplitude of the initial disturbance is kept constant at $A = 0.07$. As a result, the energy of the initial disturbance increases as the horizontal scales increase. This gives rise to stronger breakdown and larger turbulent spots. When the scales are increased further, the localized disturbance breaks down to several turbulent spots and this is not desired in this study. The next approach is to keep the initial energy of the disturbance constant, while varying the horizontal scales. The streamwise scale is varied from 7 to 11 with steps of 1 and the spanwise scale is varied form 4 to 7 with steps of 0.5. The energy level is set to $E_0 = 6.2$, the value that the disturbance with horizontal scales $l_x = l_z = 7$ assumes with the amplitude $A = 0.07$. A clear optimum can be found and among the simulated cases, $l_x = 10$ and $l_z = 5.5$ give rise to the maximum disturbance energy at time 200. The energy evolution until this instant is somewhat different for the various cases and no clear trend can be distinguished apart from the initial transient growth. When evaluating the disturbance energy at $t = 30$, 40 and 50, the maximum moves out from the considered scales towards longer and narrower initial disturbances. However, these narrow localized disturbances do not lead to transition despite their large initial amplitude.

Breuer & Haritonidis (1990) compared the numerical results for a weak localized disturbance with experiments, where the disturbance was caused by the impulsive motion of a membrane at the wall and received good qualitative agreement of the initial evolution. Henningson *et al.* (1993) investigated the effects caused by turning the localized disturbance in an angle around the y-axis and found that a non-zero angle gives rise to larger initial growth. In a preliminary study to the present work, it was found that a disturbance with a 20° angle to the free-stream direction results in lower threshold amplitudes. However, in the present study, we focus on localized disturbances aligned with the free-stream direction and that can be experimentally reproduced with the down–up motion of a membrane at the wall.

3. Results

3.1. *Transition thresholds for a localized disturbance*

In this section, the threshold amplitudes for transition from a localized disturbance to a turbulent spot are investigated in several direct numerical simulations. If the initial amplitude of the disturbance exceeds a certain threshold value, A_T, transition occurs. Previous investigations have mainly been concerned with determining the negative exponent γ, relating to the initial amplitude of the primary disturbance as $A_T \propto Re^{\gamma}$. Trefethen *et al.* (1993) used simple models to feed transient growth by nonlinearities and conjectured that for the Navier–Stokes equations, γ must be $\leqslant -1$. Baggett & Trefethen (1997) reviewed several mathematical models of transition in parallel shear flows collected from different research groups, and found the exponents $-3 \leqslant \gamma \leqslant -1$ depending on model and base flow. However, they conclude that for actual flows in pipes (e.g. Hof, Juel & Mullin 2003) and channels, the range is more likely to be

Re	A	E_0	$L_x \times L_y \times L_z$	$N_x \times N_y \times N_z$	Transition
367	0.1	8.92	$200 \times 30 \times 64$	$400 \times 201 \times 256$	No
368	0.1	8.92	$200 \times 30 \times 64$	$400 \times 201 \times 256$	Yes
500	0.044	1.76	$300 \times 19 \times 60$	$600 \times 129 \times 240$	No
500	0.045	1.81	$300 \times 19 \times 60$	$600 \times 129 \times 240$	Yes
800	0.021	0.394	$300 \times 15 \times 40$	$960 \times 161 \times 256$	No
800	0.0215	0.413	$300 \times 15 \times 40$	$960 \times 161 \times 256$	Yes
1200	0.0123	0.135	$300 \times 10 \times 40$	$1440 \times 161 \times 384$	No
1200	0.0124	0.136	$300 \times 10 \times 40$	$1440 \times 161 \times 384$	Yes

TABLE 2. Flow and box parameters for threshold simulations.

$-2 \leqslant \gamma < -1$. Most investigations dealing with this relationship focus on plane channel flows (Kreiss, Lundbladh & Henningson 1994; Lundbladh, Henningson & Reddy 1994; Dauchot & Daviaud 1995; Reddy *et al.* 1998). However, Levin *et al.* (2005) investigated transition thresholds for periodic disturbances in the ASBL at the same Reynolds numbers as considered in the present work.

There has been little work on growing boundary layers, mainly because of the difficulties of defining such a relationship, as the local Reynolds number changes with the boundary-layer thickness. However, tools for transition prediction in boundary layers have been developed for half a century. Andersson, Berggren & Henningson (1999) proposed a relation for bypass transition prediction in the Blasius boundary layer where the level of free-stream turbulence that leads to transition scales as Re^{-1}. A good correlation to this result was obtained experimentally by Fransson, Matsubara & Alfredsson (2005).

For a parallel boundary layer such as the ASBL, where the Reynolds number based on the boundary-layer thickness is constant along the streamwise direction, the procedure to find the threshold amplitude is straightforward. Simulations are carried out with a number of different initial amplitudes of the localized disturbance at the Reynolds numbers 500, 800 and 1200. The parameters for the simulations closest to the threshold amplitudes are summarized in table 2.

When evaluating whether transition occurs or not, the disturbance energy, extreme values of velocity and vorticity components and visual examinations of the flow field are taken into account. Figure 2 shows the evolution of disturbance energy (figure 2*a*), minimum and maximum wall-normal disturbance velocity (figure 2*b*) and maximum streamwise vorticity (figure 2*c*) for three initial amplitudes close to the threshold value at $Re = 500$. In this case, transition occurs for the amplitudes $A = 0.045$ and 0.046, but not for 0.044 for which the disturbance energy and flow extreme values decay after the initial transient growth.

The circles in figure 3 summarize the amplitude thresholds for the localized disturbances (LD) for the three Reynolds numbers. The thresholds are taken as the lowest amplitudes of the initial wall-normal disturbance velocity for which transition is attained in the DNS before the time $t = 1000$. The curves are least-squares fits of $A_T \propto Re^{\gamma}$ to the data and for this range of Reynolds numbers, the threshold amplitude is found to scale as $Re^{-1.5}$. This can be compared to the threshold exponents of $\gamma = -1.3$ and -1.05 for oblique waves (OW) and streamwise vortices (SV), respectively. The data from Levin *et al.* (2005) is represented by squares in figure 3.

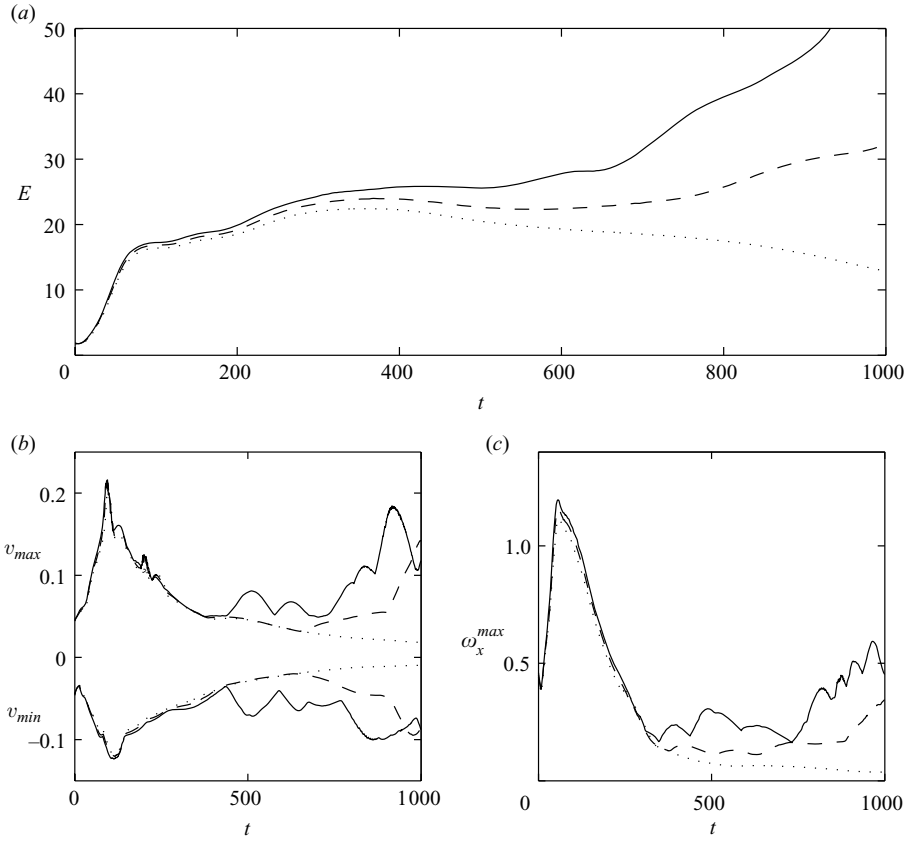

FIGURE 2. Evolution of disturbance energy (a), minimum and maximum wall-normal disturbance velocity (b) and maximum streamwise vorticity (c) at $Re = 500$ and $A = 0.046$ (solid line), 0.045 (dashed line) and 0.044 (dotted line).

In this investigation, only one type of localized disturbance is introduced in the flow, thus the obtained amplitude thresholds must be considered as an upper bound, since more optimal disturbance configurations that would lead to transition for lower initial amplitudes may exist. Furthermore, no conclusions of the asymptotic behaviour ($Re \to \infty$) can be drawn. In fact, Chapman (2002) used an asymptotic analysis of the Navier–Stokes equations to study threshold exponents for transition in plane Couette flow and plane Poiseuille flow and found discrepancies to available results from numerical simulations. He explains this difference by the fact that the asymptotic values are only reached for very large Reynolds numbers, of order 10^6, where the scaling laws of the transient growth are different than for the Reynolds numbers used in the numerical simulations. However, the present results give a good indication of the thresholds for relevant Reynolds numbers in real applications (see e.g. Schrauf 2004).

An attempt at finding the critical Reynolds number for transition initiated by the localized disturbance is also carried out. Simulations are performed with an initial amplitude of the localized disturbance of 0.1 and various Reynolds numbers, (table 2). This amplitude is considered to be sufficiently large to represent the search for a critical Reynolds number after evaluation of simulations with larger amplitudes. Relaxation of the localized disturbance appears for $Re = 367$ or below. This value

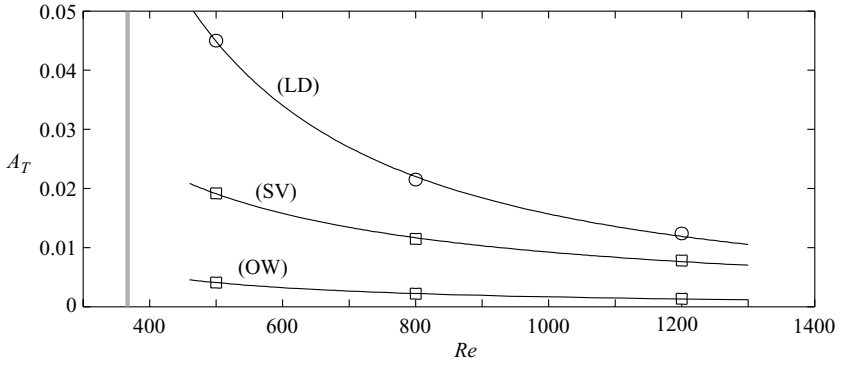

FIGURE 3. Threshold amplitude as a function of Reynolds number. The circles correspond to the lowest amplitudes of the localized disturbances (LD) from the DNS that lead to transition. Numerical data from Levin *et al.* (2005) for streamwise vortices (SV) and oblique waves (OW) are represented by the squares. The black lines are the least-squares fits to the data and the grey line indicates the critical Reynolds number of 367.

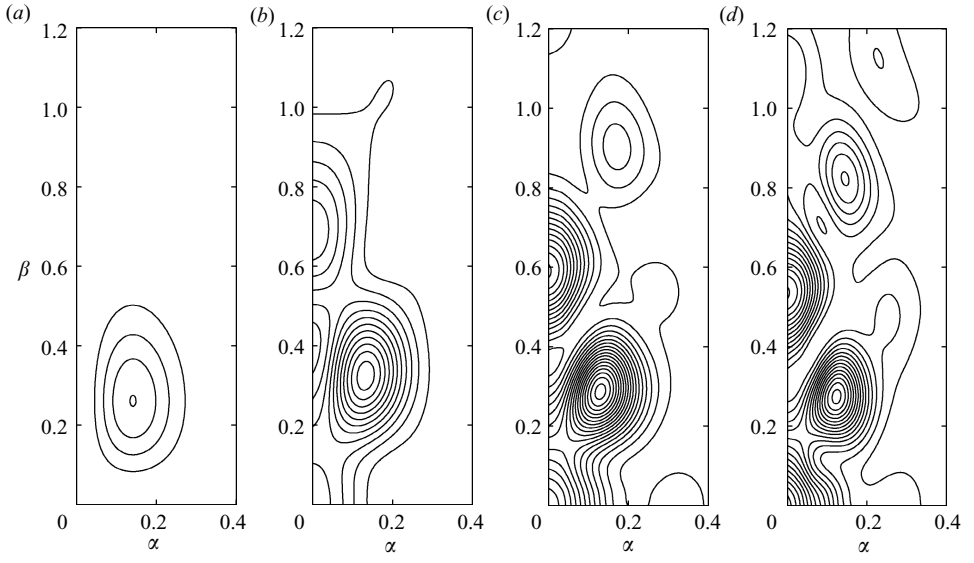

FIGURE 4. Energy spectra in Fourier space of a localized disturbance with $A = 0.06$ at $Re = 500$. (*a*) $t = 0$, (*b*) 40, (*c*) 80 and (*d*) 120. The energy is averaged in the wall-normal direction and the contours are equidistant with the same increment in all figures.

is indicated in figure 3 as the thick grey line and should also be considered as an upper bound. This critical Reynolds number says nothing about whether the turbulence is sustained or not. However, Mariani *et al.* (1993) performed DNS of the asymptotic suction turbulent boundary layer and reported sustained turbulence for a corresponding Reynolds number as low as 278.

3.2. *Breakdown to a turbulent spot*

In this section, the breakdown mechanism of a localized disturbance is discussed and visualized. In figure 4, the energy spectra of the localized disturbance at four time instants are displayed in Fourier space where α and β denote the wavenumbers in the streamwise and spanwise directions, respectively. The initial disturbance (figure 4*a*)

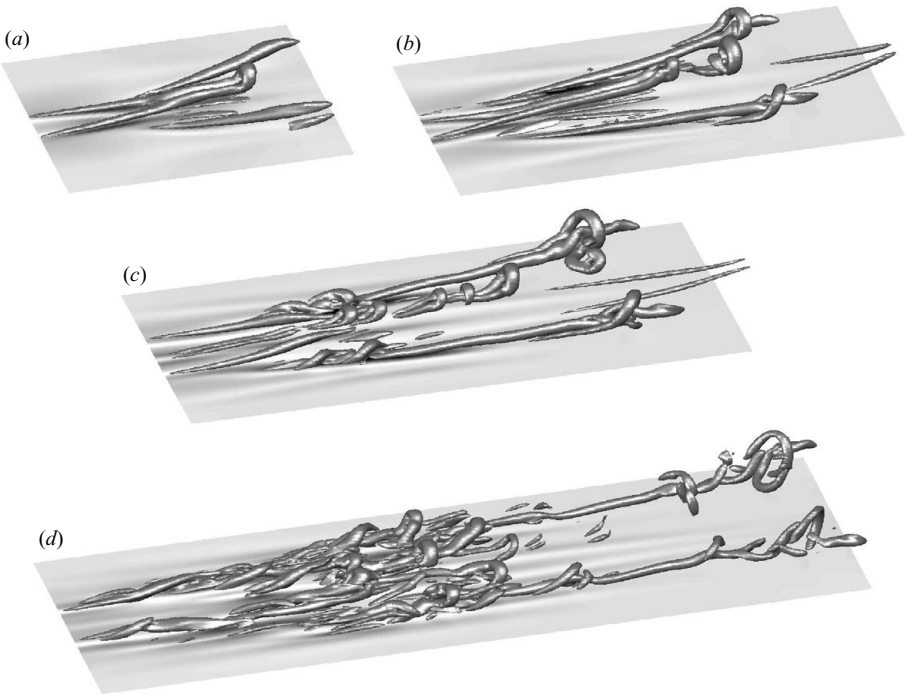

FIGURE 5. Visualizations of vortical structures ($\lambda_2 = -0.002$) and wall-shear stress (with dark regions displaying high shear) for the breakdown of a localized disturbance with $A = 0.06$ at $Re = 500$. (*a*) $t = 80$, (*b*) 140, (*c*) 200 and (*d*) 300. The scales in all figures are equidistant and the width is 40.

is centred around a pair of oblique waves (the negative part is not showed). As time proceeds (figure 4*b–d*), a β-cascade (Henningson *et al.* 1993) takes place, where energy is transferred to higher wavenumbers along the β-axis. The mechanism behind this β-cascade is the nonlinear interaction between the modes present in the disturbance and can be understood by looking at the convolution sums in Fourier space.

The turbulent spot is an assemblage of many small-scale streaky structures and hairpin vortices (Perry *et al.* 1981; Sankaran *et al.* 1988; Singer & Joslin 1994; Schröder & Kompenhans 2004). These hairpin vortices evolve at the trailing edge of the young spot and increase the region of turbulence in the streamwise and spanwise directions as the spot grows. The spot appears to grow through the birth of new structures rather than the growth or spreading of the substructures themselves. Vortical structures can be identified in the flow by plotting regions where the second largest eigenvalue λ_2 of the Hessian of the pressure assumes negative values (Jeong *et al.* 1997). Figure 5 shows a sequence of the early development of the localized disturbance with $A = 0.06$ at $Re = 500$. The initial disturbance develops into a hairpin vortex aligned with the streamwise direction, see figure 5(*a*) which shows the instant at $t = 80$. Its legs are close to the wall at the trailing edge of the disturbance while the head is located higher up and further downstream. Between the legs, an upward motion is present. On each side of the head, counter-rotating structures can be seen. Figure 5(*b*) shows the instant at $t = 140$, the head is detached as a result of vortex stretching and a new head is formed in its place. At the same time, spiral vortices appear at the counter-rotating structures on each side. An instability is developing on the stretched legs of the hairpin vortex that breaks up into several

Re	A	$L_x \times L_y \times L_z$	$N_x \times N_y \times N_z$	Number of points	End time
500	0.06	$400 \times 25 \times 100$	$800 \times 181 \times 400$	57.9 million	1200
800	0.03	$400 \times 12 \times 80$	$1280 \times 129 \times 512$	84.5 million	950
1200	0.02	$300 \times 10 \times 80$	$1440 \times 161 \times 768$	178 million	800

TABLE 3. Flow and box parameters for simulations of turbulent spots.

individual hairpin vortices and at $t = 200$, six hairpin heads can be distinguished along the centreline in figure 5(c). At $t = 300$, the flow pattern has become complex with many hairpin and spiral vortices characterizing a young turbulent spot.

3.3. *Development of turbulent spots*

In this section, turbulent spots are visualized and the spreading angles and propagation velocities of the leading and trailing edges are evaluated. Table 3 summarizes the parameters for the three simulations performed. Apart from the localized disturbance, random noise is added to the initial velocity field in order to break up symmetries. The level of the noise is prescribed with its energy density, which has the value 10^{-7} for all three simulations.

3.3.1. *Overall features*

As the spot propagates downstream, it grows in size. However, the wall-normal spreading is very small. Figure 6 shows the turbulent spots at $t = 800$. The streamwise disturbance velocity is visualized with dark and light regions displaying high and low values, respectively. The spot for the Reynolds number 500 is shown in figures 6(a) and 6(b) where the wall-parallel plane at $y = 1$ is shown in figure 6(a) and the (x, y)-plane along the centreline ($z = 0$) is shown in figure 6(b). Figures 6(c) and 6(d) show a corresponding visualization of the turbulent spot for Reynolds number 800. In figures 6(e) and 6(f), the turbulent spot for Reynolds number 1200 is shown. For all visualizations, the length of the planes is 300 while the width and height show the entire spanwise and wall-normal extent of the computational box, respectively. From the visualizations, it can be interpreted that the turbulent spot takes a bullet-shaped form with a rounded leading edge and a straight trailing edge. This shape becomes more distinct for higher Reynolds numbers as the scales within the spot become smaller. The interior of the spot is occupied by turbulent streaky structures. The side views reveal that the leading edge develops an overhang over the laminar flow and this is typical for turbulent spots in boundary layers. Beneath this overhang, long streaks extend from the turbulent region close to the wall. These streaks evolve from the influence of the disturbed flow in the overhang region. Behind the trailing edge of the spot, shorter streaks persist and they evolve from the relaminarization of turbulent structures propagating at a slower rate than the trailing edge itself.

In the laminar flow surrounding the spot, a large-scale flow is induced. In the wake of the spot, the flow is accelerated close to the wall, resulting in a calm region similar to that seen behind turbulent spots in boundary layers without wall suction. The flow on the sides of the widest part of the spot, is also weakly accelerated, while the flow on the sides behind that region and beside the wake is weakly decelerated. As expected for such a stable base flow, no evidence of waves surrounding the spot can be seen. The deviation of the laminar flow induced by the large-scale flow surrounding the spot typically decays exponentially with the distance from the spot (see e.g. Schumacher & Eckhardt 2001). In order to study the laminar exterior on the sides of the turbulent

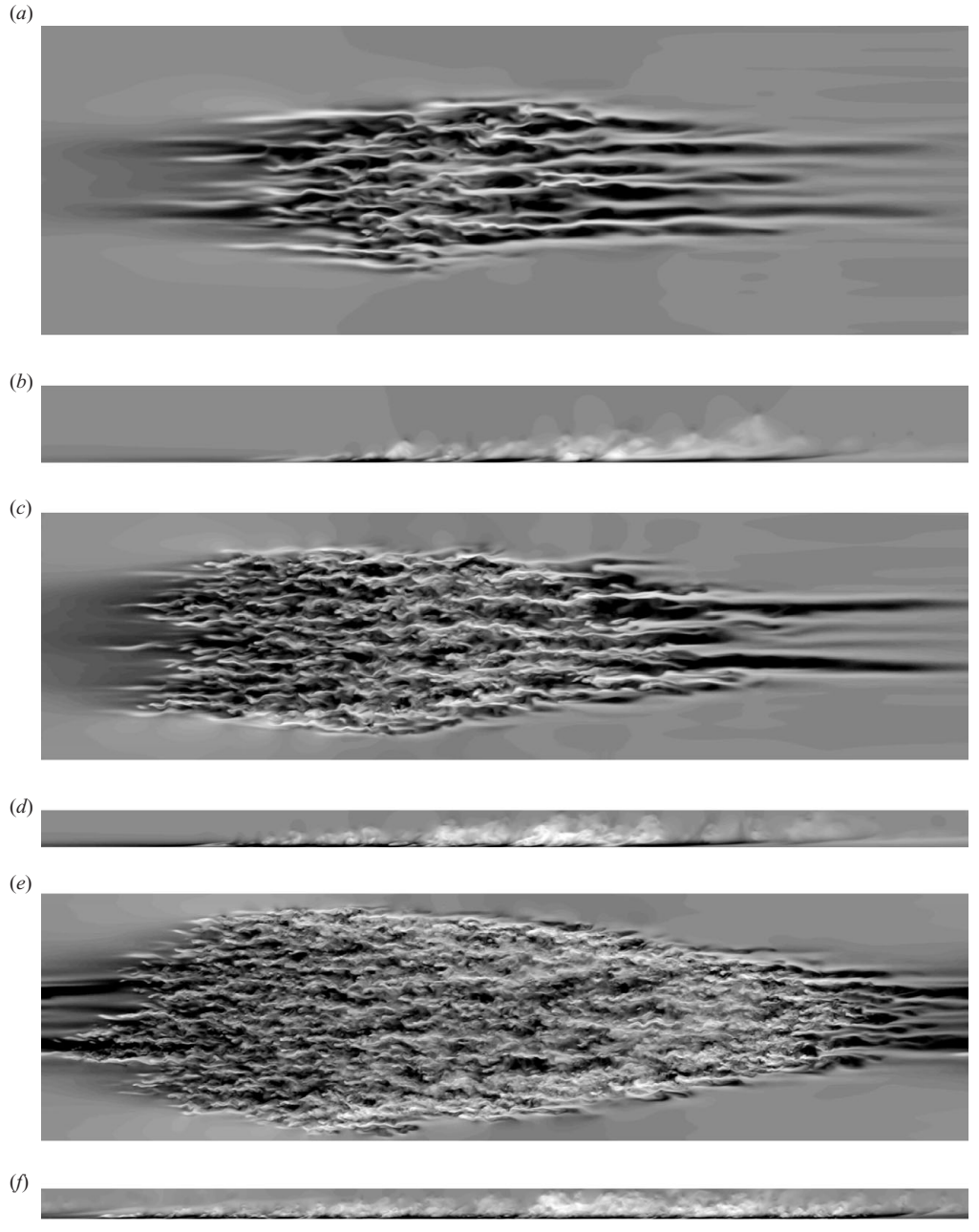

FIGURE 6. Visualizations of turbulent spots at $t = 800$. Dark and light regions show high and low streamwise disturbance velocity, respectively. Flow is from left to right and the length of the planes is 300. (a, c, e) Wall-parallel plane at $y = 1$. (b, d, f) (x, y)-plane through the centre line of the spots ($z = 0$). (a, b) $Re = 500$. (c, d) $Re = 800$. (e, f) $Re = 1200$.

spot at $Re = 500$, an additional simulation was performed with a box of length and width 200. Figure 7 shows the disturbance energy, averaged in the wall-normal direction, along the spanwise direction originating from the centre of the turbulent spot at $t = 400$. The expected exponential decay of the flow distortion can be seen.

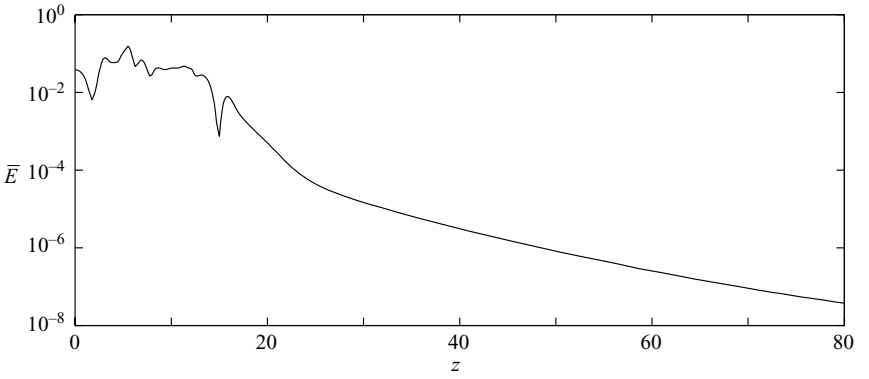

FIGURE 7. Disturbance energy along the spanwise direction originating from the centre of a turbulent spot at $Re = 500$ and $t = 400$. The energy is averaged in the wall-normal direction.

3.3.2. *Spreading characteristics*

In order to evaluate the spreading rate of the turbulent spot in the wall-parallel plane at $y = 1$, the streamwise derivative of the streamwise velocity provides a well-defined measure. The region of turbulence is represented by the criteria $\partial u/\partial x \geqslant 0.05$, which agrees well with other similar conditions as well as visual examinations of the wall-parallel planes in figures 6. This condition is chosen because it is easy to measure in an experiment and it filters away the laminar streaks. For the evaluation of the spreading rates, the initial evolution of the spots is disregarded. In agreement with spots in other flows, the length and the width of the turbulent spots assume a linear growth. A closer look at the propagation of the leading and trailing edges for $Re = 500$ reveals that the individual structures, in the considered plane, propagate in a slower rate than the leading and trailing edges themselves. New turbulent structures are born in the laminar streaks preceding the turbulent region and at the trailing edge, structures move out of the spot and undergo relaminarization. The data from the lateral spreading are more scattered since the widest part of the spots move back and forth somewhat as new structures are born. It should also be mentioned that the spreading differs on the two sides owing to the randomness introduced by the initial noise.

The main characteristics of the spreading of the three simulated spots are summarized in figure 8. As can be seen in figure 8(*a*), the velocity of the leading edge increases slightly with increased Reynolds number, but seems to level off at a value of 0.9 for high Reynolds numbers and this value is in agreement with the turbulent spot in the flat-plate boundary layer. The trailing-edge velocity, on the other hand, decreases almost linearly with increasing Reynolds number for the considered Reynolds numbers. The half-width angle, which is taken as the mean value from both sides, increases with increasing Reynolds number (figure 8*b*). In this figure, the cross indicates the reasonable assumption of a zero spreading angle at the critical Reynolds number.

As the spot grows linearly in length and width, and the wall-normal growth is negligible in comparison, it is reasonable to expect a quadratic growth of the disturbance energy in the fully developed turbulent spot. To assess whether this is true or not, the square root of the disturbance energy is plotted versus time in figure 9(*a*). Linear fits to the data are represented by the grey lines and confirm the assumption of a quadratic growth of the disturbance energy. The agreement becomes better for higher Reynolds numbers. An explanation for this is that the turbulent structures

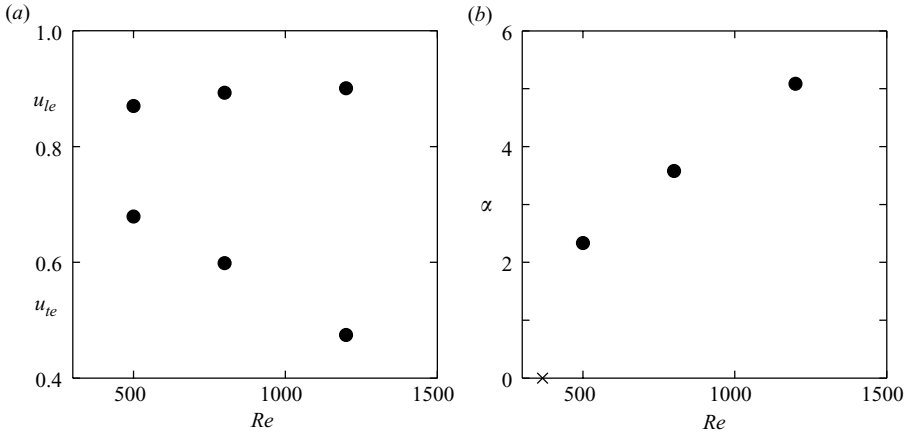

FIGURE 8. Spreading of turbulent spots versus Reynolds number. (*a*) Propagation velocities, u_{le} and u_{te}, of the leading and trailing edges, respectively. (*b*) Mean half-width angle α. The cross indicates the critical Reynolds number.

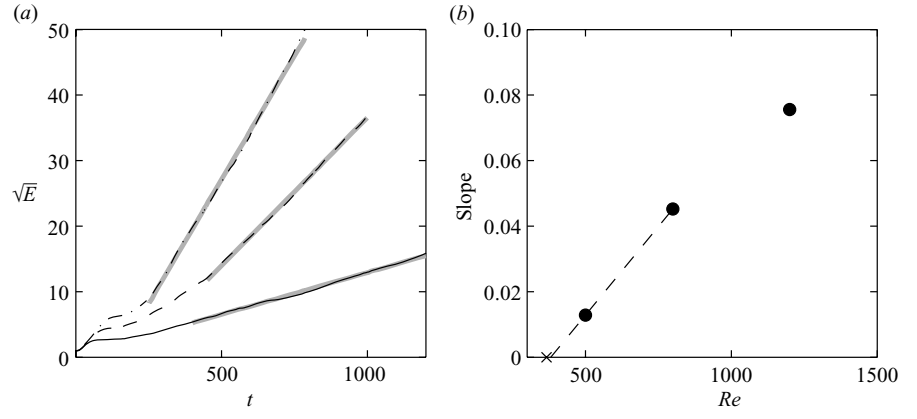

FIGURE 9. Evolution of the disturbance energy within turbulent spots. (*a*) Square root of the energy versus time for $Re = 500$ (—), 800 (— — —) and 1200 (— · —). Grey lines are linear fits to the data within the plotted intervals. (*b*) Slopes of the fitted lines versus Reynolds number. The cross indicates the critical Reynolds number.

within the spot are larger for lower Reynolds numbers, and hence, the evolution of the energy is more affected by the growth or decay of individual structures. In figure 9(*b*), the slopes of the fitted lines are plotted versus Reynolds number. If we assume a linear increase of the slope with increasing Reynolds number for $Re \leqslant 800$ (dashed line), the Reynolds number for a zero growth of the disturbance energy falls very close to the critical Reynolds number found in § 3.1. This might provide an additional approach for finding an approximation of the critical Reynolds number for the onset of a turbulent spot.

4. Summary and conclusion

A study of the development of localized disturbances and turbulent spots in the asymptotic suction boundary layer are carried out using direct numerical simulations. The localized disturbance is superposed to the initial velocity field in the form of two counter-rotating vortex pairs. This type of initial disturbance can be reproduced

experimentally with the down–up motion of a membrane located at the wall (Breuer & Haritonidis 1990). A parametric study of the horizontal scales of the initial disturbance is performed. It is found that keeping the initial disturbance energy constant rather than the initial disturbance amplitude is appropriate when comparing the growth of disturbances with different scales. The disturbance scales that lead to the highest growth under the conditions investigated are used in the simulations.

The threshold amplitude for breakdown of the localized disturbance into a turbulent spot is investigated for the Reynolds numbers $Re = 500$, 800 and 1200, based on the free-stream velocity and the displacement thickness. It is found that the threshold amplitude, defined as the maximum wall-normal velocity of the initial disturbance, scales as $Re^{-1.5}$ for the considered Reynolds numbers. This can be compared to the numerical results of Levin *et al.* (2005), who found that the threshold amplitude scales as $Re^{-1.3}$ for oblique transition and as $Re^{-1.05}$ for transition initiated by streamwise vortices and random noise. Furthermore, a search for the critical Reynolds number for breakdown of the localized disturbance is carried out. It is found that for $Re \leqslant 367$, the localized disturbance decays after the initial transient growth.

The vortical structures within the early breakdown mechanism of the localized disturbance are studied for $Re = 500$. The initial disturbance develops into a hairpin vortex aligned with the streamwise direction. Its legs are close to the wall at the trailing edge of the disturbance while the head is located higher up and further downstream. This head is detached as a result of vortex stretching and a new head is formed in its place. An instability that develops on the original hairpin vortex further feeds this process, resulting in a row of hairpin vortex heads. In a previous numerical study (Singer & Joslin 1994), the same behaviour was found in the flat-plate boundary layer. The young turbulent spot consists of many hairpin and spiral vortices that increase the size of the spot through the addition of new structures.

The shape and spreading rate of the turbulent spot are determined for $Re = 500$, 800 and 1200. Flow visualizations reveal that the turbulent spot takes a bullet-shaped form with a rounded leading edge and a straight trailing edge. This shape becomes more distinct for higher Reynolds numbers as the scales within the spot diminish. The leading edge develops an overhang over the laminar flow. Beneath this overhang, long streaks extend from the turbulent region close to the wall and the breakdown of these streaks is responsible for the streamwise growth of the spot. Behind the trailing edge of the spot, shorter streaks persist and evolve from turbulent structures that move in a slower rate than the trailing edge itself. The spot is followed by a calm wake with accelerated flow. No evidence of waves surrounding the spot exists.

The fully developed turbulent spot is found to grow linearly both in length and width while the wall-normal spreading is very small. As a result, the disturbance energy within the spot assumes a quadratic growth, which becomes more legible for higher Reynolds numbers. The leading edge is found to propagate at about 85–90 % of the free-stream velocity while the trailing-edge velocity decreases with increasing Reynolds number. The half-width angle is found to increase with increasing Reynolds number. However, the spreading rates of the turbulent spot have to level off to constant values at higher Reynolds numbers.

To summarize, the turbulent spot in the asymptotic suction boundary layer bears many similarities to spots in other flows. Its shape and spreading rates are reminiscent of the turbulent spot in boundary layers subjected to a favourable pressure gradient. In common with spots in plane Couette flow and plane Poiseuille flow, the spreading rates are dependent on the Reynolds number.

This work was funded by the Swedish Energy Agency (Energimyndigheten). The direct numerical simulations were performed at the Center for Parallel Computers at KTH.

REFERENCES

Alavyoon, F., Henningson, D. S. & Alfredsson, P. H. 1986 Turbulent spots in plane Poiseuille flow–flow visualization. *Phys. Fluids* **29**, 1328–1331.

Andersson, P., Berggren, M. & Henningson, D. S. 1999 Optimal disturbances and bypass transition in boundary layers. *Phys. Fluids* **11**, 134–150.

Baggett, J. S. & Trefethen, L. N. 1997 Low-dimensional models of subcritical transition to turbulence. *Phys. Fluids* **9**, 1043–1053.

Balakumar, P. & Hall, P. 1999 Optimum suction distribution for transition control. *Theoret. Comput. Fluid Dyn.* **13**, 1–19.

Bech, K. H., Henningson, D. S. & Henkes, R. A. W. M. 1998 Linear and nonlinear development of localized disturbances in zero and adverse pressure gradient boundary-layers. *Phys. Fluids* **10**, 1405–1418.

Breuer, K. S. & Haritonidis, J. H. 1990 The evolution of a localized disturbance in a laminar boundary layer. Part 1. Weak disturbances. *J. Fluid Mech.* **220**, 569–594.

Breuer, K. S. & Landahl, M. T. 1990 The evolution of a localized disturbance in a laminar boundary layer. Part 2. Strong disturbances. *J. Fluid Mech.* **220**, 595–621.

Byström, M. G., Levin, O. & Henningson, D. S. 2007 Optimal disturbances in suction boundary layers. *Eur. J. Mech.* B/*Fluids* **26**, 330–343.

Cantwell, B., Coles, D. & Dimotakis, P. 1978 Structure and entrainment in the plane of symmetry of a turbulent spot. *J. Fluid Mech.* **87**, 641–672.

Carlson, D. R., Widnall, S. E. & Peeters, M. F. 1982 A flow-visualization of transition in plane Poiseuille flow. *J. Fluid Mech.* **121**, 487–505.

Chapman, S. J. 2002 Subcritical transition in channel flows. *J. Fluid Mech.* **451**, 35–97.

Dauchot, O. & Daviaud, F. 1995 Finite amplitude perturbation and spots growth mechanism in plane Couette flow. *Phys. Fluids* **7**, 335–343.

Elder, J. W. 1960 An experimental investigation of turbulent spots and breakdown to turbulence. *J. Fluid Mech.* **9**, 235–246.

Emmons, H. W. 1951 The laminar–turbulent transition in a boundary layer. Part I. *J. Aero. Sci.* **18**, 490–498.

Fransson, J. H. M. & Alfredsson, P. H. 2003 On the disturbance growth in an asymptotic suction boundary layer. *J. Fluid Mech.* **482**, 51–90.

Fransson, J. H. M. & Corbett, P. 2003 Optimal linear growth in the asymptotic suction boundary layer. *Eur. J. Mech.* B/*Fluids* **22**, 259–270.

Fransson, J. H. M., Matsubara, M. & Alfredsson, P. H. 2005 Transition induced by free-stream turbulence. *J. Fluid Mech.* **527**, 1–25.

Griffith, A. A. & Meredith, F. W. 1936 The possible improvement in aircraft performance due to boundary layer suction. *Tech. Rep.* 2315. Rep. Aero. Res. Coun.

Henningson, D. S. & Alfredsson, P. H. 1987 The wave structure of turbulent spots in plane Poiseuille flow. *J. Fluid Mech.* **178**, 405–421.

Henningson, D. S. & Kim, J. 1991 On turbulent spots in plane Poiseuille flow. *J. Fluid Mech.* **228**, 183–205.

Henningson, D. S., Spalart, P. & Kim, J. 1987 Numerical simulations of turbulent spots in plane Poiseuille and boundary-layer flow. *Phys. Fluids* **30**, 2914–2917.

Henningson, D. S., Lundbladh, A. & Johansson, A. V. 1993 A mechanism for bypass transition from localized disturbances in wall-bounded shear flows. *J. Fluid Mech.* **250**, 169–238.

Hocking, L. M. 1975 Non-linear instability of the asymptotic suction velocity profile. *Q. J. Mech. Appl. Maths* **28**, 341–353.

Hof, B., Juel, A. & Mullin, T. 2003 Scaling of the turbulence transition threshold in a pipe. *Phys. Rev. Lett.* **91**, 244502.

Jeong, J., Hussain, F., Schoppa, W. & Kim, J. 1997 Coherent structures near the wall in a turbulent channel flow. *J. Fluid Mech.* **332**, 185–214.

Joslin, R. D. 1998 Aircraft laminar flow control. *Annu. Rev. Fluid Mech.* **30**, 1–29.

Katz, Y., Seifert, A. & Wygnanski, I. 1990 On the evolution of the turbulent spot in a laminar boundary layer with a favourable pressure gradient. *J. Fluid Mech.* **221**, 1–22.

Kreiss, G., Lundbladh, A. & Henningson, D. S. 1994 Bounds for threshold amplitudes in subcritical shear flows. *J. Fluid Mech.* **270**, 175–198.

Levin, O., Davidsson, E. N. & Henningson, D. S. 2005 Transition thresholds in the asymptotic suction boundary layer. *Phys. Fluids* **17**, 114104.

Lundbladh, A. & Johansson, A. V. 1991 Direct simulation of turbulent spots in plane Couette flow. *J. Fluid Mech.* **229**, 499–516.

Lundbladh, A., Berlin, S., Skote, M., Hildings, C., Choi, J., Kim, J. & Henningson, D. S. 1999 An efficient spectral method for simulation of incompressible flow over a flat plate. *Tech. Rep.* KTH, Department of Mechanics, Stockholm.

Lundbladh, A., Henningson, D. S. & Reddy, S. C. 1994 Threshold amplitudes for transition in channel flows. In *Transition, Turbulence, and Combustion* (ed. M. Y. Hussaini, T. B. Gatski & T. L. Jackson), vol. 1, pp. 309–318. Kluwer.

Mariani, P., Spalart, P. & Kollmann, W. 1993 Direct simulation of a turbulent boundary layer with suction. In *Near-Wall Turbulent Flows* (ed. R. M. C. So, C. G. Speziale & B. E. Launder), pp. 347–356. Elsevier.

Mathew, J. & Das, A. 2000 Direct numerical simulations of spots. *Current Sci.* **79**, 816–820.

Nordström, J., Nordin, N. & Henningson, D. S. 1999 The fringe region technique and the Fourier method used in the direct numerical simulation of spatially evolving viscous flows. *SIAM J. Sci. Comput.* **20**, 1365–1393.

Perry, A. E., Lim, T. T. & Teh, E. W. 1981 A visual study of turbulent spots. *J. Fluid Mech.* **104**, 387–405.

Pralits, J. O., Hanifi, A. & Henningson, D. S. 2002 Adjoint-based optimization of steady suction for disturbance control in incompressible flows. *J. Fluid Mech.* **467**, 129–161.

Reddy, S. C., Schmid, P. J., Baggett, J. S. & Henningson, D. S. 1998 On stability of streamwise streaks and transition thresholds in plane channel flows. *J. Fluid Mech.* **365**, 269–303.

Riley, J. J. & Gad-el-Hak, M. 1985 The dynamics of turbulent spots. In *Frontiers in Fluid Mechanics* (ed. S. H. Davis & J. L. Lumley), pp. 123–155. Springer.

Sankaran, R., Sokolov, M. & Antonia, R. A. 1988 Substructures in a turbulent spot. *J. Fluid Mech.* **197**, 389–414.

Schrauf, G. 2004 Large-scale laminar-flow tests evaluated with linear stability theory. *J. Aircraft* **41**, 224–230.

Schröder, A. & Kompenhans, J. 2004 Investigation of a turbulent spot using multi-plane stereo particle image velocimetry. *Exps. Fluids* **36**, 82–90.

Schumacher, J. & Eckhardt, B. 2001 Evolution of turbulent spots in a parallel shear flow. *Phys. Rev.* E **63**, 046307.

Seifert, A. & Wygnanski, I. J. 1995 On turbulent spots in a laminar boundary layer subjected to a self-similar adverse pressure gradient. *J. Fluid Mech.* **296**, 185–209.

Singer, B. A. 1996 Characteristics of a young turbulent spot. *Phys. Fluids* **8**, 509–521.

Singer, B. A. & Joslin, R. D. 1994 Metamorphosis of a hairpin vortex into a young turbulent spot. *Phys. Fluids* **6**, 3724–3736.

Tillmark, N. & Alfredsson, P. H. 1992 Experiments on transition in plane Couette flow. *J. Fluid Mech.* **235**, 89–102.

Trefethen, L. N., Trefethen, A. E., Reddy, S. C. & Driscoll, T. A. 1993 Hydrodynamic stability without eigenvalues. *Science* **261**, 578–584.

Wygnanski, I., Sokolov, M. & Friedman, D. 1976 On a turbulent 'spot' in a laminar boundary layer. *J. Fluid Mech.* **78**, 785–819.

Wygnanski, I., Haritonidis, J. H. & Kaplan, R. E. 1979 On a Tollmien–Schlichting wave packet produced by a turbulent spot. *J. Fluid Mech.* **92**, 505–528.

Yoshioka, S., Fransson, J. H. M. & Alfredsson, P. H. 2004 Free stream turbulence induced disturbances in boundary layers with wall suction. *Phys. Fluids* **16**, 3530–3539.

Zuccher, S., Luchini, P. & Bottaro, A. 2004 Algebraic growth in a Blasius boundary layer: optimal and robust control by mean suction in the nonlinear regime. *J. Fluid Mech.* **513**, 135–160.